A Parameter Alternating VSG Controller of VSC-MTDC Systems for Low Frequency Oscillation Damping

Weiyu Wang, *Student Member, IEEE,* Lin Jiang, *Member, IEEE,* Yijia Cao, *Senior Member, IEEE,* Yong Li, *Senior Member, IEEE*

***Abstract*—The virtual synchronous generator (VSG) has been widely applied for mimicking the dynamic performance of a synchronous generator (SG) by power-electronic interfaced power sources. When the VSG is implemented in VSC-based multi-terminal direct current (VSC-MTDC) systems, the impact of VSG on both ac- and dc-grid dynamics, i.e., the low frequency oscillatory (LFO) modes and dc voltage stability should be taken into consideration. This paper investigates the participation of the VSG controller in low frequency oscillatory (LFO) modes and the impact on dc voltage stability. The influence of VSG parameters on the system dynamics is investigated by the Singular Value Decomposition (SVD) analysis and modal analysis. A parameter alternating VSG (AVSG) controller is proposed to improve the damping performance to LFO modes and mitigating the negative impact of VSG on dc voltage stability. The effectiveness of the proposed AVSG controller is validated according to the non-linear simulations on two test systems.**

***Index Terms*—Virtual synchronous generator (VSG), voltage source converter (VSC), multi-terminal direct current system (MTDC), inter-area oscillation damping, dc voltage stability.**

I. Introduction

TO transmit the electric power from the remote renewable energy sources (RES) to the load centre, VSC-based high voltage direct current (VSC-HVDC) system is considered to be a promising solution due to its high cost-efficiency and flexible power regulation [1], [2]. To improve the power-sharing between multiple RESs and asynchronous ac systems, several point-to-point VSC-HVDC links can be connected to form a meshed dc grid, i.e., VSC-based multi-terminal HVDC (VSC-MTDC) system. However, a surge of RESs onto a power system could lead to the reduction of grid inertia as power electronic-interfaced RESs have little or even no rotating mass [3]. Such a low inertia power system is prone to an excessive rate of change of frequency (ROCOF) and severe frequency deviation if the demand for electric power spikes.

Virtual synchronous generator (VSG) has been proposed to control the power electronic interfaced RES for enhancing the grid inertia. The idea of VSG was first proposed in the European project "VSYNC" [4]. The VSG emulates the inertial responses of SGs by incorporating the swing equation into the active power control loop [5]–[7]. The virtual inertia response of VSG-controlled VSCs can restrain the rate of change of frequency (ROCOF) and provide frequency support for power systems. However, the VSG introduce two major challenges when it is applied in VSC-MTDC systems.

$Challenge\ 1$: Oscillation issue. Resulting from the similar swing characteristic to SGs, the active power output of the VSG may oscillate after grid disturbance [8], [9]. The oscillatory characteristic of VSG could affect the original oscillatory modes of power systems. For VSC-MTDC systems, the VSG has a more prominent influence on oscillatory modes because: 1) the VSC-stations have similar capacity level of SGs; (2) multiple VSC-stations could be integrated into the same ac grid. Thus the VSG could interact with SGs, especially in the low frequency range [10]. It is important to investigate the impact of VSG on the low frequency oscillations (LFO) when it is implemented in VSC-MTDC systems.

$Challenge\ 2$: DC voltage stability. The ability of the VSG to emulate virtual inertia is achieved by the integrator in the active power loop of VSC-stations, which reduces the power regulation speed of VSC-stations [11]. Thus, the power deficiency in the dc network is hard to be compensated in time and could further lead to a large dc voltage deviation after disturbances in dc network. VSC-MTDC systems employing VSG have more difficulties to maintain the dc voltage stability.

Implementation of VSG in high voltage power systems has been investigated in [10], [12], [13]. In [10], the damping torque analysis is utilized to understand the influence of VSG-controlled VSC-HVDC systems on LFO modes and the phase compensation method is employed to promote the damping performance of VSG-controlled VSC-HVDC system. In [12], a unified VSG is proposed for VSC-MTDC systems to improve the stability of very weak ac grids. In [13], impedance analysis and Nyquist stability criterion are utilized to improve the stability of the weak ac grids via VSG-based VSC-HVDC.

For real synchronous generators (SG), the inertia constant is determined by the rotational kinetic energy stored in the rotor at rated speed. One cannot change the inertia constant of real SGs unless the physical components of SGs are replaced. Thus, the inertia constant of real SGs can be considered to be unchangeable during the transient period. However, the VSG controller is realized by the control algorithm, whose parameters can be adjusted in real time to improve the controller performance. The VSG has three key parameters,

This work was supported in part by the national Natural Science Foundation of China (NSFC) under Grant 61233008 and 51520105011, in part by the 111 Project under Grant B17016. (Corresponding authors: Yijia Cao and Yong Li.)

W. Wang, Y. Cao and Y. Li are with the College of Electrical and Information Engineering, Hunan University, Changsha, 410082, China, (e-mail: victor0125@hnu.edu.cn, yjcaohnu@163.com, yongli@hnu.edu.cn).

L. Jiang is with the Department of Electrical Engineering and Electronics, University of Liverpool, Liverpool L69 3GJ, U.K. (e-mail: ljiang@liv.ac.uk).

i.e., the virtual inertia, governor droop coefficient and damping factor. To improve the dynamic performance of VSG in real-time, parameter alternating methods are proposed to adjust the key parameters of VSG according to the operation state of power systems [14]–[18]. For example, large virtual inertia is desired to restrain the ROCOF caused by load variation, whereas a small one is needed to mitigate the oscillatory characteristic of VSG. In [8], a linear control theory-based oscillation damping approach is proposed for VSG to damp the output power oscillation. In [15] and [16], a VSG with the alternating moment of inertia (AMI) is proposed to damp the power oscillation and secure the angular stability of the microgrids. However, the proposed bang-bang control only switches the virtual inertia between a small and a large value. In [14], the proposed VSG can search the optimal parameters online to minimize the frequency deviation and ROCOF. In [17], [18], both the virtual inertia and damping factor are changed during the transient period to improve the damping of VSG controllers.

The existing methods are essential to understand the influence of VSG on oscillatory modes and guide the online parameter adjustment. However, the aforementioned references only investigated the single VSG, and the impact of VSG parameters on low frequency oscillatory modes had not been discussed. The influence of VSG controllers on dc voltage dynamics is also ignored as it is usually assumed that there is a large dc power source. In this paper, the impact of the VSG controller on both ac- and dc-side dynamics is investigated according to a four-terminal dc grid connecting with an inter-area ac grid. A parameter alternating VSG controller (AVSG) is proposed for VSC-MTDC systems to dampen LFO modes. The main contributions can be concluded as follows:

1) The participation of the classical VSG controller in LFO modes is revealed by modal analysis;
2) The impact of VSG parameters, i.e, the virtual inertia time constant H_v, the virtual governor droop coefficient $K_{v\omega}$ and the dc voltage droop coefficient K_{vv}, on the LFO modes and the dc voltage dynamics are investigated by the Singular Value Decomposition (SVD) analysis and modal analysis;
3) A smooth parameter alternating law of VSG is proposed to enhance the damping of low frequency oscillations. DC voltage stability can be secured if LFO modes are sufficiently dampened.

The rest of the paper is organized as follows. In Section II, the linearized model of a hybrid AC/DC power system with VSG controllers is presented. In Section III, the impact of VSG on dc voltage dynamics and LFO modes are investigated by SVD analysis and modal analysis. In Section IV, the proposed AVSG is elaborated step by step. Section V and VI verify the effectiveness of the proposed AVSG by nonlinear simulations in DIgSILENT/PowerFactory. Section VII concludes the findings of this paper.

II. Linearlized Model of Hybrid AC/DC Power Systems

A typical 4-terminal VSC-MTDC system connecting with a two-area ac grid and two stiff ac grids is shown in Fig. 1. VSC1 and VSC2 employ the VSG controller and operate in the inverter mode, whereas VSC3 and VSC4 adopt the classical $P-V$ droop control and operate in rectifier mode.

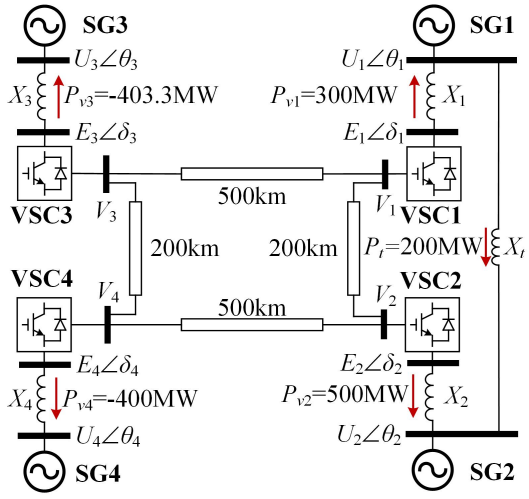

Fig. 1. Test system.

A. Linearized Model of VSC-stations

The dynamic processes of VSC-stations can be investigated by the detailed model considering the switching details [19], [20]. However, the detailed model is hard to be applied in the electromechanical-transient analysis due to the excessive computational burden. In this paper, the equivalent averaged-value model (AVM) of VSC-stations is employed, which can accurately predict the dynamic behavior of VSC from the output perspective and improves the computational efficiency [21]–[23]. The AVM of a VSC-station can be modeled by a controlled current source in the dc-side and as a controlled voltage source in the ac-side, as shown in Fig. 2. Neglecting the switching-losses of VSC-stations, the active power output of VSC-stations P_v is assumed to be equal to the power injected from the dc network. Thus, the dynamics of VSC-stations can be represented as

$$\begin{cases} \Delta\dot{V}_{eq,i} = \dfrac{1}{C_{eq,i}}(\Delta I_i - \Delta I_{o,i}) \\ \Delta\dot{I}_i = \dfrac{1}{L_i}(\Delta V_i - \Delta V_{eq,i} - R_i\Delta I_i) \\ \Delta\dot{V}_i = \dfrac{1}{C_{l,i}}(\Delta I_{in,i} - \Delta I_i) \\ \Delta I_{o,i} = \dfrac{\Delta P_{v,i}}{V_{eq0,i}} - \dfrac{P_{v0,i}}{V_{eq0,i}^2}\Delta V_{eq,i} \\ \Delta I_{in,i} = \sum\limits_{j\in N_i}\Delta I_{l,ij} \end{cases} \tag{1}$$

where the subscript "i" represents the VSC-stations i; C_{eq} denotes the equivalent dc-link capacitor of VSC-stations; V is the dc voltage of VSC-stations; R and L represent the aggregated resistance and inductance, which is given by $R=(2/3)R_{arm}$ and $L=(2/3)L_{arm}$, where R_{arm} and L_{arm} are the equivalent resistance and inductance of one arm; $C_{l,i}$ is the equivalent dc cable capacitance at dc terminal of VSC-station i; $I_{in,i}$ is

the dc current injected by the dc grid; $I_{l,ij}$ are the dc current through the dc cable between node i and j; N_i is the set of the neighbors of terminal i in the dc grid.

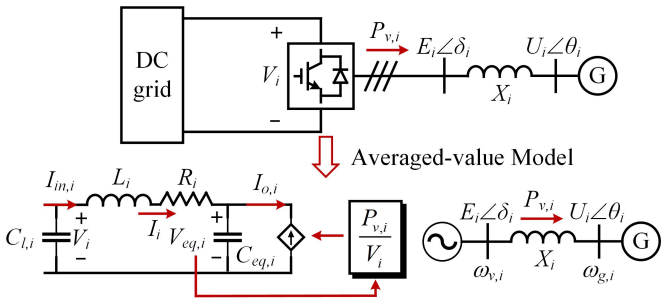

Fig. 2. The single line diagram of the AVM of VSC-staitons.

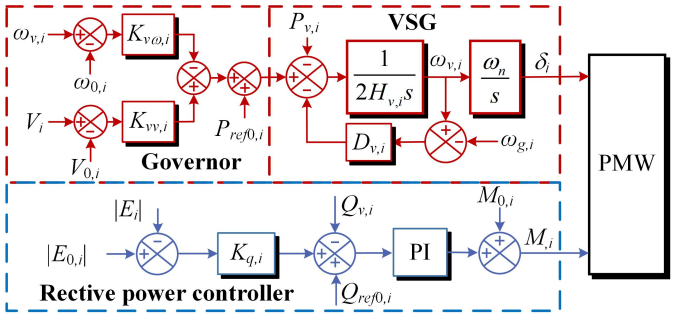

Fig. 3. The block diagram of classical VSG controller.

The active power output P_v and the ac-terminal voltage $E\angle\delta$ of VSC-stations are dominated by the controllers, which are introduced in the following subsections.

1) VSG Controller: Fig. 3 shows the block diagram of the basic VSG controller. The VSG controlled VSC-stations is equivalent to voltage sources, which can emulate the inertia response of real synchronous generators (SG) by regulating the active power output [6], [8]. Since only the active power control loop of VSG controller is of interest, the reactive power controller is not modeled and the voltage magnitude E is fixed to the initial value E_0. The virtual rotor speed ω_v and phase angle δ can be obtained by the swing equation

$$\begin{cases} \Delta\dot{\omega}_{v,i} = \dfrac{1}{2H_{v,i}}[\Delta P_{ref,i} - \Delta P_{v,i} - D_{v,i}(\Delta\omega_{v,i} - \Delta\omega_{g,i})] \\ \Delta\dot{\delta}_i = \omega_s \Delta\omega_{v,i} \\ \Delta P_{v,i} = T_{v,i}(\Delta\delta - \Delta\theta) \end{cases} \tag{2}$$

where ω_g is the grid angular frequency; H_v and D_v are the virtual inertia time constant and damping coefficient, respectively; ω_s is the nominal angular frequency in rad/s; T_v is the synchronizing torque coefficients, which is calculated by $\frac{E_{0,i}U_{0,i}}{X_i}\cos(\delta_{0,i} - \theta_{0,i})$, X is the aggregated reactance of the converter transformer and phase reactors.

The virtual governor (VGOV) is composed of $P-\omega$ and $P-V$ droop characteristics

$$\Delta P_{ref,i} = \Delta P_{ref0,i} + K_{vv,i}\Delta V_i - K_{v\omega,i}\Delta\omega_{v,i} \tag{3}$$

where K_{vv} and $K_{v\omega}$ are the $P-V$ and $P-\omega$ droop coefficients. Note that the ω_g in the damping term $D_{v,i}(\Delta\omega_{v,i} - \Delta\omega_{g,i})$ in (2) is a measured signal, which can be replaced by the constant value ω_0 = 1p.u. [24]. The different form of the damping term, i.e., $D_{v,i}(\Delta\omega_{v,i} - \Delta\omega_{g,i})$ and $D_{v,i}(\Delta\omega_{v,i} - \Delta\omega_{0,i})$ can lead to different dynamic performance of VSG controller [25]. In this paper, $D_{v,i}(\Delta\omega_{v,i} - \Delta\omega_{0,i})$ is adopted. Thus, the damping term of the virtual swing equation is equivalent to the $P-\omega$ droop characteristic of the virtual governor. To combine the effect of the virtual governor and damping term, only the effect of $K_{v\omega}$ will be discussed and D_v is set to 0.

2) $P-V$ Controller: The VSC-stations with $P-V$ droop controller are modeled in dq-frame, which is composed of $P-V$ droop characteristic, power and current controller. The current controller with the converter plant can be simplified as Low Pass Filters (LPF) with small time constant T_c [26]. When VSC-stations connect to strong ac grids, the reactive power controller can be ignored as it has limited influence on active power transfer [21]. Thus, only the d-axis control loop is considered. The dynamics of the active power control loop can be described as

$$\begin{cases} \Delta\dot{\phi}_i = \Delta P_{ref,i} - \Delta P_{v,i} \\ \Delta\dot{I}_{d,i} = \dfrac{1}{T_{c,i}}(\Delta I_{dref,i} - \Delta I_{d,i}) \\ \Delta P_{ref,i} = \Delta P_{ref0,i} + K_{v,i}\Delta V_i \\ \Delta I_{dref,i} = K_{P,i}(\Delta P_{ref,i} - \Delta P_{v,i}) + K_{I,i}\Delta\phi_i \\ \Delta P_{v,i} = I_{d0,i}\Delta E_{d,i} + E_{d0,i}\Delta I_{d,i} \end{cases} \tag{4}$$

where K_v is the $P-V$ droop coefficient; ϕ is a state variable representing the state of the integral part in the outer control loop; K_P and K_I are the proportional and integral coefficients of outer PI controller, respectively; E_d is the ac-terminal voltage of VSC-stations in d-axis. Assume that the phase-locked loop is fast enough to ensure that the d-axis is always aligned with the ac-terminal voltage, i.e., $E_d = |E|$, and then $\Delta P_{v,i} = E_{d0,i}\Delta I_{d,i}$.

B. Linearized Model of DC Networks

The dc cable dynamics can be modeled by an equivalent π model, which is given as

$$\begin{cases} \Delta\dot{V}_{l,i} = \dfrac{1}{C_{l,i}}\displaystyle\sum_{j\in N_i}\Delta I_{l,ij} \\ \Delta\dot{I}_{l,ij} = \dfrac{1}{L_{l,ij}}(\Delta V_{l,i} - \Delta V_{l,j} - R_{l,ij}\Delta I_{l,ij}) \end{cases} \tag{5}$$

where V_l is the node voltage in the dc network; C_l represents the equivalent dc cable capacitance; $I_{l,ij}$ are the dc current through the dc cable between node i and j; R_l and L_l are the equivalent dc cable resistance and inductance.

C. Linearized Model of AC Grids

The ac grids are represented by the classical second-order generator model considering the dynamics of speed-governor

and non-reheat turbine.

$$\begin{cases} \Delta\dot{\omega}_{g,i} = \dfrac{1}{2H_{g,i}}(\Delta P_{m,i} - \Delta P_{g,i} - D_{g,i}\Delta\omega_{g,i}) \\ \Delta\dot{\theta}_i = \omega_s \Delta\omega_{g,i} \\ \Delta\dot{Y}_i = -\dfrac{K_{\omega,i}}{T_{g,i}}\Delta\omega_{g,i} - \dfrac{1}{T_{g,i}}\Delta Y_i \\ \Delta\dot{P}_{m,i} = \dfrac{1}{T_{ch,i}}\Delta Y_i - \dfrac{1}{T_{ch,i}}\Delta P_{m,i} \end{cases} \tag{6}$$

where θ and ω_g denote the rotor angle and speed of SGs; H_g and D_g represent the inertial time constant and damping coefficient, respectively; P_m and P_g are the mechanical and electrical power, respectively; K_ω is the speed droop coefficient; Y is the valves/gate position of turbines; T_g and T_{ch} are the time constant of governor and turbine, respectively.

The active power flow of ac grids has the following relationship

$$\begin{cases} \Delta P_{g,1} = \Delta P_t - \Delta P_{v1} + \Delta P_{lod,1} \\ \Delta P_{g,2} = -\Delta P_t - \Delta P_{v2} + \Delta P_{lod,2} \\ \Delta P_{g,i} = -\Delta P_{v,i4} + \Delta P_{lod,i}, i = 3,4 \\ \Delta P_t = T_t(\Delta\theta_1 - \Delta\theta_2) \end{cases} \tag{7}$$

where P_{lod} and P_t are the load demand and the active power transmitted by the transmission line, respectively; T_t are the synchronizing torque coefficients, which can be calculated by $\frac{U_{0,1}U_{0,2}\cos(\theta_{0,1}-\theta_{0,2})}{X_t}$, respectively.

D. State-Space Model of the Hybrid AC/DC Power System

To investigate the system dynamics, the $y_v = [\Delta V_1 \dots \Delta V_4]^T$ and $y_\omega = [\Delta\omega_{g,1} \dots \Delta\omega_{g,4}]^T$ are chosen as the output vectors, and $u = [\Delta P_{ref0,1} \dots \Delta P_{ref0,4}]^T$ and $d = [\Delta P_{lod,1} \dots \Delta P_{lod,4}]^T$ are chosen as the control input vector and the disturbance input vector. Rearranging (1)−(7) yields the state-space model of the test system

$$\begin{cases} \dot{x} = Ax + Bu + B_d d \\ y_v = C_v x \\ y_\omega = C_\omega x \end{cases} \tag{8}$$

where x are the vector of state variables; A, B, B_d, C_v, and C_ω are the state matrix, input matrix, disturbance matrix, and output matrix of dc voltage and frequency, respectively.

To validate the state-space model of the hybrid ac/dc power system shown in Fig. 1, a step change $\Delta P_{lod,1}$ =1p.u. is applied at t = 0.5s. The system responses are shown in Fig. 4. The system parameters used for the simulation are given in Table I. The state-space model is built in Matlab by m-code and the non-linear simulation is performed in DIgSILENT/PowerFactory.

It can be observed from Fig. 4 that the responses of state-space model (blue dotted lines) agree well with that of nonlinear model (red solid lines). Hence, the proposed state-space model is verified.

TABLE I
PARAMETERS OF THE TEST SYSTEM

VSC-stations	DC Network
S_n = 800MVA	R_l = 0.0114Ω/km
V_n = 800kV, V_{acn} = 220kV	L_l = 0.9356mH/km
C = 100μF, L_{arm} = 45mH	C_l = 0.0123μF/km
VSG and $P-V$ Parameters	**AC Grids**
H_v = 3s, $K_{v\omega}$ = 20p.u.	$S_{g,1} = S_{g,2}$ = 900MVA
K_{vv} = 20p.u., D_v = 0	$S_{g,3} = S_{g,4}$ = 1800MVA
K_v = 20p.u., K_P = 2p.u.	H_g = 6.5s, K_ω = 20p.u.
K_I = 20p.u., T_c = 0.001s	X = 12.123Ω, X_t = 48.492Ω

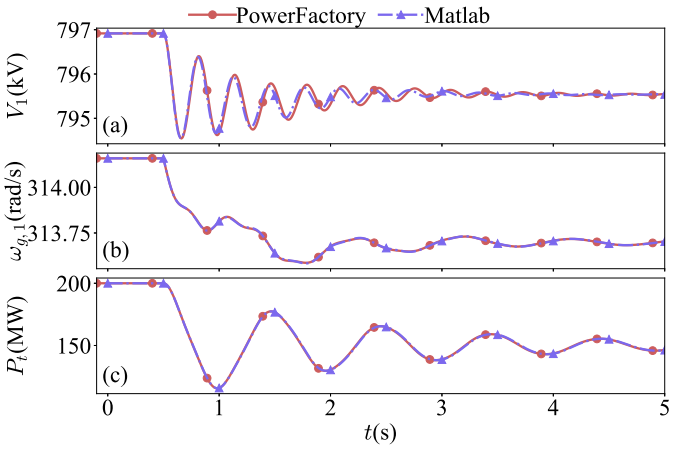

Fig. 4. System responses obtained from non-linear and linear models. (a) the dc voltage of VSC1; (b) the rotor speed of SG1; (c) the active power on transmission line.

III. INFLUENCE OF VSG CONTROLLER ON SYSTEM DYNAMICS

When the VSG controller is implemented in VSC-MTDC systems, the impact of the VSG controller on both the ac- and dc-side dynamics must be carefully examined. In this section, Singular Value Decomposition (SVD) analysis and modal analysis are used to investigate the system dynamics with different VSG numbers and different parameters.

A. Singular Value Decomposition

Consider a constant $l \times m$ complex matrix M. M can be decomposed into its SVD:

$$M = U\Sigma V^H \tag{9}$$

where U and V are the $l \times l$ and $m \times m$ unit orthonormal matrix, respectively; $\Sigma = \begin{bmatrix} \Sigma_1 & 0 \\ 0 & 0 \end{bmatrix}$ is a $l \times m$ matrix. V^H is conjugate transpose of V. Σ_1 is a diagonal matrix containing the singular value $\sigma_1 \dots \sigma_q$ arranged in a descending order, where $q = \min\{l, m\}$. The column vector elements of U and V, i.e., u_i and v_i, are the output and input singular vectors, which yields

$$Mv_i = \sigma_i u_i \tag{10}$$

Equation (10) indicates that if an input vector is in the direction of v_i, the output vector will be in the direction u_i and the corresponding gain of the vector length is σ_i. The largest

gain for any input direction is equal to the maximum singular value σ_1, i.e.,

$$\max_{v\neq 0}\frac{\|Mv\|_2}{\|v\|_2}=\frac{\|Mv_1\|_2}{\|v_1\|_2}=\sigma_1\triangleq\bar{\sigma} \tag{11}$$

where $\|\cdot\|_2$ is the Euclidian norm.

For Multi-input Multi-output systems (MIMO), SVD is an effective tool to identify the frequencies at which the system is prone to dynamic problems [27], [28]. To apply the SVD in system dynamic analysis, the transfer matrix needs to be obtained from the state-space model (8) first

$$G(s)=[G_{vd}(s)\ G_{\omega d}(s)] \tag{12}$$

where G_{vd} is the transfer matrix between y_v and d; $G_{\omega d}$ is the transfer matrix between y_ω and d. G_{vd} and $G_{\omega d}$ are given by

$$\begin{cases}G_{vd}(s)=C_v(sI-A)^{-1}B_d\\ G_{\omega d}(s)=C_\omega(sI-A)^{-1}B_d\end{cases} \tag{13}$$

Then the singular value of G_{vd} and $G_{\omega d}$ at any frequency can be obtained by substituting s with $j\omega$. For any disturbance input vector d, the gain of G_{vd} and $G_{\omega d}$ at frequency ω has the following relationship

$$\begin{cases}\underline{\sigma}_v\leq\dfrac{\|G_{vd}(j\omega)d\|_2}{\|d\|_2}\leq\bar{\sigma}_v\\ \underline{\sigma}_{\omega,k}\leq\dfrac{\|G_{\omega d}(j\omega)d\|_2}{\|d\|_2}\leq\bar{\sigma}_\omega\end{cases} \tag{14}$$

The maximum singular value $\bar{\sigma}_v$ and $\bar{\sigma}_\omega$ indicate the largest deviation gain of dc voltage and frequency. Thus, Bode plots of $\bar{\sigma}_v$ and $\bar{\sigma}_\omega$ over a specific frequency range can evaluate the system dynamics.

To investigate the system dynamics with different VSG numbers, three cases are considered, which are given in Table II and Fig. 5.

TABLE II
STUDY CASES

Case	VSG	$P-V$
A	VSC#1	VSC#2 − #4
B	VSC#1 and #2	VSC#3 and #4
C	VSC#1 − #3	VSC#4

It can be observed from Fig. 5(a) that with more VSG controllers applied in the test system, the overall dc voltage deviation is increased and the peaks of $\bar{\sigma}_v$ at around 3.2Hz are boosted whilst the peak of $\bar{\sigma}_v$ at 1.08Hz is reduced (Case B and C). Fig. 5(b) indicates that if VSC1 and VSC2 employ the VSG controller, the peak of $\bar{\sigma}_\omega$ at 1.08Hz can be reduced. However, the peak of $\bar{\sigma}_\omega$ is not reduced when VSC3 is equipped with a VSG controller (Case C) because VSC3 is not integrated into the two-area ac grid. Thus, with more VSG controllers applied in VSC-MTDC systems, the ac grid frequency stability can be improved but the dc voltage stability is weakened. In the following part of this section, Case B is used to investigate the system dynamics with different VSG parameters.

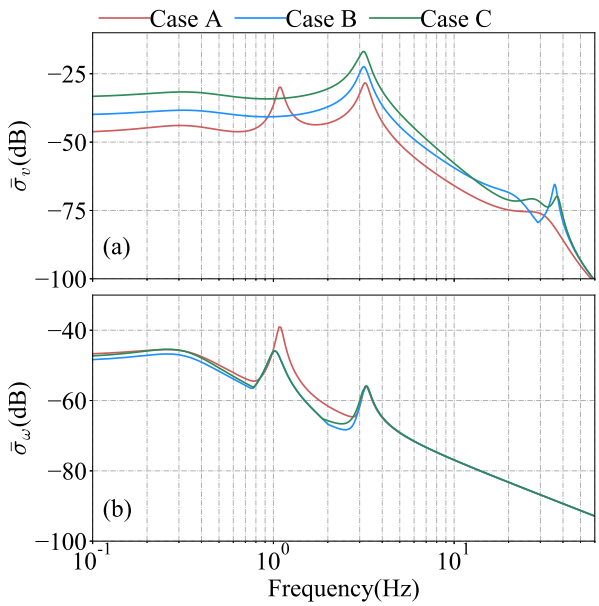

Fig. 5. Maximum singular value of G_{vd} and $G_{\omega d}$ with different cases.

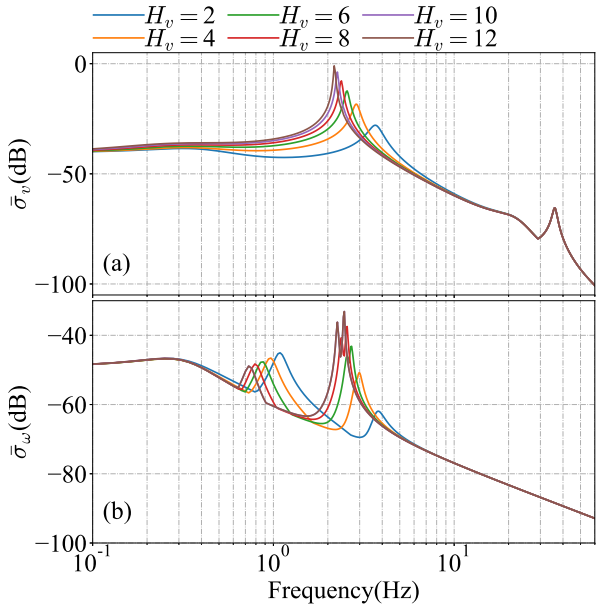

Fig. 6. Maximum singular value of G_{vd} and $G_{\omega d}$ with different H_v.

Bode plots of $\bar{\sigma}_v$ and $\bar{\sigma}_\omega$ with different H_v, $K_{v\omega}$ and K_{vv} shown in Figs. 6 and 7.

Firstly, only H_v is changed from 1−12s, and $K_{v\omega}$ and K_{vv} are set to 20p.u. and 0p.u., respectively. Fig. 6 shows that the peak of $\bar{\sigma}_v$ is encouraged greatly by increasing H_v, which means that the disturbances in ac grids may trigger serious dc voltage dynamic issues due to the VSG controller. The peak of $\bar{\sigma}_\omega$ at 1.08Hz is attenuated whilst a relatively higher frequency resonant is boosted significantly, which indicates that VSG controllers with large H_v could weaken the system stability. Then, $K_{v\omega}$ is increased from 10−120p.u., and H_v and K_{vv} are set to 10s and 0p.u., respectively. Both the peaks of $\bar{\sigma}_v$ and $\bar{\sigma}_\omega$ are significantly decreased, as shown in Fig.

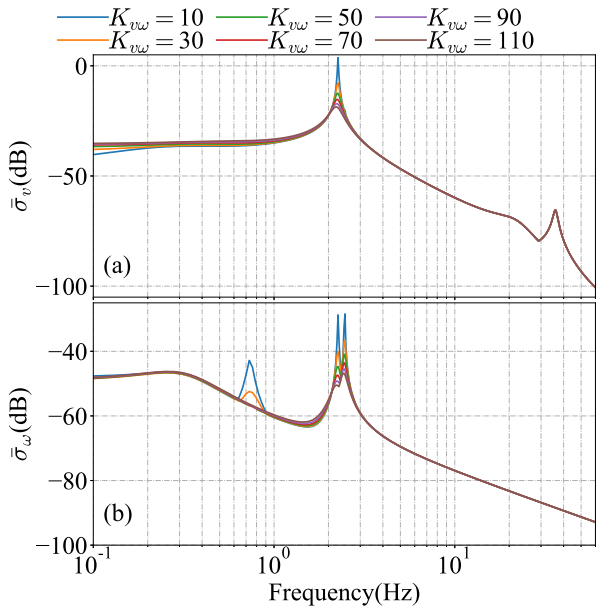

Fig. 7. Maximum singular value of G_{vd} and $G_{\omega d}$ with different $K_{v\omega}$.

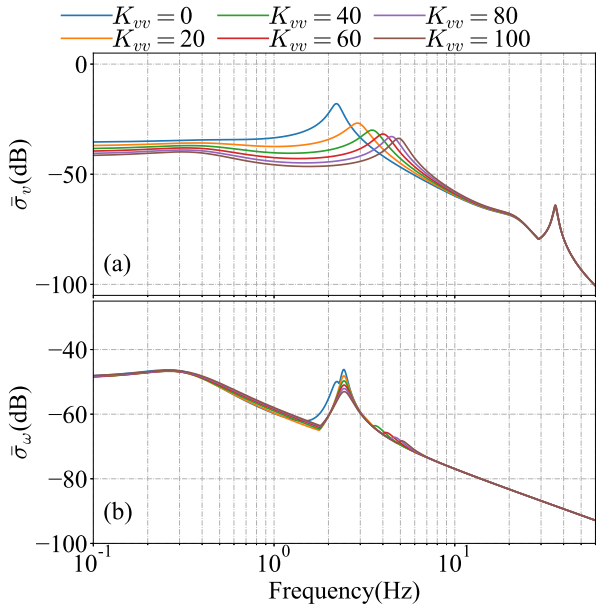

Fig. 8. Maximum singular value of G_{vd} and $G_{\omega d}$ with different K_{vv}.

7. Thus, the stability of hybrid ac/dc power systems can be enhanced by a large $K_{v\omega}$. However, the dc voltage deviation in low frequency (<1Hz) is slightly magnified. Next, K_{vv} is increased from 0−20p.u., and H_v and $K_{v\omega}$ are set to 10s and 100p.u., respectively. The peak of $\bar{\sigma}_v$ can be further reduced whilst $\bar{\sigma}_\omega$ is slightly influenced, as shown in Fig. 8. This phenomenon suggests that the $P-V$ droop control of the virtual governor (3) can reduce the dc voltage deviation.

B. Modal Analysis

To further investigate the influence of VSG parameters on system oscillatory modes, modal analysis is performed based on the Case B. The modes whose damping ratio is lower than 0.1 and oscillatory frequency is lower than 3Hz are chosen as the critical ones, as shown in Table III.

TABLE III
CRITICAL OSCILLATORY MODES

Mode number	Eigenvalues	Mode Shape
λ_{12}&λ_{13}	-0.534 ± 6.381j	{SG1,VSC1}⟺{SG2,VSC2}
λ_{17}&λ_{18}	-1.169 ± 19.883j	SG1⟺VSC1 SG2⟺VSC2
λ_{19}&λ_{20}	-1.06 ± 20.346j	SG1⟺VSC1 SG2⟺VSC2

It can be observed that VSC1 and VSC2, which are equipped with VSG controllers, participate in three critical LFO modes. One is a inter-area mode and others are local modes. The influence of VSG parameters on these modes are revealed by the eigenvalue loci, as shown in Fig. 9.

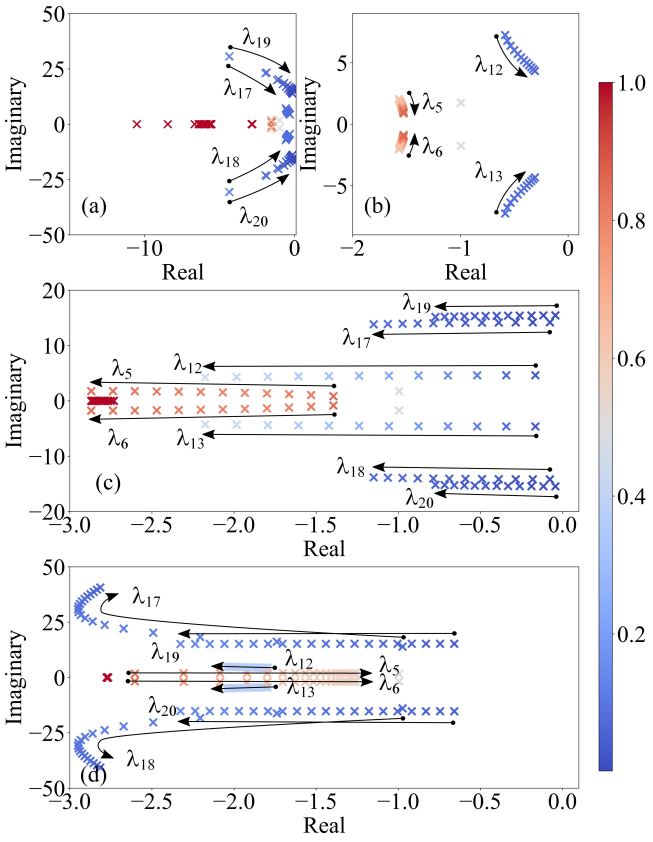

Fig. 9. The eigenvalue loci with the change of different parameters of VSG.

Firstly, H_v is changed from 1−12s, and let $K_{v\omega}=20$p.u. and $K_{vv}=0$p.u. Fig. 9 (a) and (b) indicate that all the critical oscillatory modes migrate toward the original point monotonously by increasing H_v, which means that both the damping ratios and oscillatory frequencies of the critical modes are reduced. It should be noted that the damping ratio of a well-damped mode (λ_5&λ_6) is enhanced by increasing H_v. Then $K_{v\omega}$ is increased from 10−120p.u, and H_v and K_{vv} are set to 10s and 0p.u., respectively. As can be observed from Fig. 9(c), the critical LFO modes move toward the left-half plane

(LHP) monotonously by increasing $K_{v\omega}$, which indicates that the damping ratio of all the critical modes are significantly enhanced. Next K_{vv} is increased from 0 to 200p.u., and let $H_v = 10s$ and $K_{v\omega} = 100$p.u. In contrast to H_v and $K_{v\omega}$, the change of K_{vv} has a complex influence on the critical LFO modes. One can observed from Fig. 9(d) that the damping ratio of the oscillatory modes $\lambda_{12}\&\lambda_{13}$, $\lambda_{17}\&\lambda_{18}$ and $\lambda_{19}\&\lambda_{20}$ are improved with the increase of K_{vv}. Whilst the damping of $\lambda_5\&\lambda_6$ are decreased because of the migration to the right-half plane (RHP). Note that the damping ratio of $\lambda_{17}\&\lambda_{18}$ will be reduced after reaching the inflection points.

IV. Design of the VSG for Low Frequency Oscillation Damping

In this section, a parameter alternating law is designed for VSG controllers to improve the system damping to LFO modes and mitigate the negative influence on dc voltage. In [15]–[18], the virtual moment of inertia J_v, which is equivalent to the inertia constant H_v, is changed to improve the damping performance of VSG controllers. However, as discussed in Section III, increasing virtual inertia H_v can severely weaken the system damping to LFO modes and both the resonant peaks of dc voltage and frequency are encouraged. Thus, only $K_{v\omega}$ and K_{vv} can be adjusted whereas H_v should be constant during the transient period.

Since the VSC-stations controlled by VSG controllers could participate in LFOs, the virtual rotor speed ω_v and dc voltage could oscillate around the nominal point when disturbances occur. Thus, $d\omega_v/dt$ and ΔV are used to indicate the disturbed states. The general parameter alternating strategy are given as follows:

a) If $|d\omega_v/dt| > |d\omega_v/dt|_t$, where $|d\omega_v/dt|_t$ is the threshold of $|d\omega_v/dt|$, $K_{v\omega}$ should be increased because large $K_{v\omega}$ can reduce both the resonant peaks of dc voltage and frequency, and strengthen the damping of critical LFO modes;
b) If $|\Delta V| > |\Delta V|_t$, where $|\Delta V|_t$ is the threshold of $|\Delta V|$, K_{vv} should be increased because large K_{vv} can restrain the dc voltage deviation.

To smoothly change $K_{v\omega}$ and K_{vv}, the sigmoid function $S(x)$ is employed to design the parameter alternating law. The sigmoid function $S(x)$ is described as

$$S(x) = \frac{S_{\max} - S_{\min}}{1 + e^{-k_r(x-x_0)}} + S_{\min} \tag{15}$$

where x is excessive $|d\omega_v/dt|$ or $|\Delta V|$; x_0 is the x-value of the sigmoid's midpoint; $S_{\max}$ and $S_{\min}$ are the lower and upper boundaries; k_r is the growth rate. Since $S(x)$ reaches the bounds only at infinity, $S'_{\max} = 0.99\frac{S_{\max}-S_{\min}}{2} + S_{\min}$ and $S'_{\min} = 0.01\frac{S_{\max}-S_{\min}}{2} + S_{\min}$ are used as the lower and upper bounds, which can be reached in a reasonable range of x, as shown in Fig .10. The design of alternating law is equivalent to find the appropriate $S'_{\max}, S'_{\min}, S_0, k_r$, and x_0 for $K_{v\omega}$ and K_{vv}.

1) Upper and Lower Bounds: The upper bound of $K_{v\omega}$ should ensure that the sum of the damping ratio of critical LFO modes can be maximized and does not exceed the steady-state $P-\omega$ droop characteristic.

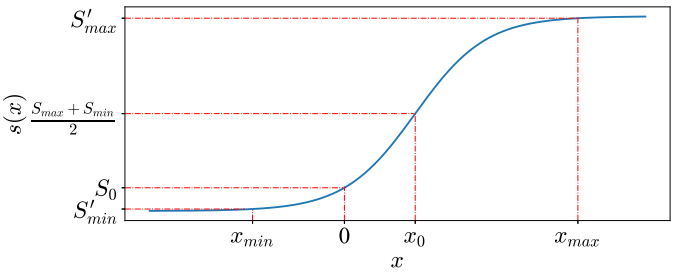

Fig. 10. Plot of Sigmoid function.

$$K_{v\omega,\max} = \min\{\arg\max_{K_{v\omega}}\{\sum_{i\in\text{LFOs}}\zeta_i\}, \frac{S_{rated}}{\Delta\omega_{\max}}\} \tag{16}$$

where ζ_i is the damping ratio of LFO mode i, S_{rated} represents the rated capacity of VSC-stations; $\Delta\omega_{\max}$ is the limit of frequency deviation provided by the Grid Codes. For example, if the limit of frequency deviation of a 50Hz power system is ± 0.5Hz, the second term of (16) is 100p.u. If the first term of (16) exceeds 100p.u., $K_{v\omega,\max}$ is set to 100p.u. The Upper bound of K_{vv} is similar to $K_{v\omega,\max}$, i.e.,

$$K_{vv,\max} = \min\{\arg\max_{K_{vv}}\{\sum_{i\in\text{LFOs}}\zeta_i\}, \frac{S_{rated}}{\Delta V_{\max}}\} \tag{17}$$

The lower bounds of $K_{v\omega}$ and K_{vv} will not be reached because $K_{v\omega}$ and K_{vv} should not be lower than the initial value. In this paper, both $K_{v\omega,\min}$ and $K_{vv,\min}$ are set to 0p.u.

2) Growth Rate k_r and x: In general, x_ω and x_v should always keep positive for increasing $K_{v\omega}$ and K_{vv} when $|d\omega_v/dt| > |d\omega_v/dt|_t$ and $|\Delta V| > |\Delta V|_t$. Thus, x_ω and x_v are given by

$$x_\omega = \begin{cases} 0 & \text{, if } |\frac{d\omega_v}{dt}| < |\frac{d\omega_v}{dt}|_t \\ |\frac{d\omega_v}{dt}| - |\frac{d\omega_v}{dt}|_t & \text{, else} \end{cases} \tag{18}$$

$$x_v = \begin{cases} 0 & \text{, if} |\Delta V| < |\Delta V|_t \\ |\Delta V| - |\Delta V|_t & \text{, else} \end{cases} \tag{19}$$

However, $|d\omega_v/dt|$ and $|\Delta V|$ are usually small in per unit. Whilst $S(x)$ is monotonously increasing from $S'_{\min}$ to $S'_{\max}$ in the domain of [-4.6, 4.6] when $k_r = 1$. Thus, x_ω and x_v need to be magnified to ensure the effective variation of $K_{v\omega}$ and K_{vv}. $k_{r\omega}$ and k_{rv} can be calculated by

$$\begin{cases} k_{r\omega} = 4.6/\left|\dfrac{d\omega_v}{dt}\right|_{\text{ea}} \\ k_{rv} = 4.6/|\Delta V|_{\text{ea}} \end{cases} \tag{20}$$

where $|d\omega_v/dt|_{\text{ea}}$ and $|\Delta V|_{\text{ea}}$ are the average value of the excessive $|d\omega_v/dt|$ and $|\Delta V|$ over the threshold $|d\omega_v/dt|_t$ and $|\Delta V|_t$ during the oscillatory period. Then k_{rh} and $k_{r\omega}$ should be further corrected by trial and error to pursue a satisfied damping performance.

3) Midpoint x_0: The midpoints $x_{\omega 0}$ and x_{v0} ensures that $K_{v\omega}$ and K_{vv} are equal to their initial value respectively when $x = 0$. Setting $x_\omega = 0$ and $x_v = 0$ in (15) yields

$$\begin{cases} x_{\omega 0} = \dfrac{1}{k_{r\omega}} \ln \dfrac{K_{v\omega,\max} - K_{v\omega 0}}{K_{v\omega 0} - K_{v\omega,\min}} \\ x_{v0} = \dfrac{1}{k_{rv}} \ln \dfrac{K_{vv,\max} - K_{vv0}}{K_{vv0} - K_{vv,\min}} \end{cases} \tag{21}$$

4) Completed parameter adjustment laws: According to (15)−(21), the completed online parameter alternating law of H_v and K_ω are given by

$$\begin{cases} K_{v\omega} = \dfrac{K_{v\omega,\max} - K_{v\omega,\min}}{1 + e^{-k_{r\omega}(x_\omega - x_{\omega 0})}} + K_{v\omega,\min} \\ K_{vv} = \dfrac{K_{vv,\max} - K_{vv,\min}}{1 + e^{-k_{rv}(x_v - x_{v0})}} + K_{vv,\min} \end{cases} \tag{22}$$

The modal analysis performed in Section III.B indicates that the VSC-stations controlled by VSG controller can participate in multiple LFO modes, which includes both local and inter-area modes. According to (22), the proposed AVSG can adjust its key parameters, i.e., $K_{v\omega}$ and K_{vv} to dampen these LFO modes at the same time. It should be pointed out that although the AVSG controller can improve the overall damping performance, it may not provide the best damping performance to a specific mode as the sum of the damping ratios of these modes are of interest.

When LFO modes are triggered, the AVSG controller could change its key parameter by the local information. However, the variation range are determined by the modal analysis, which relies on the linearized model of power systems (8). Since the operating points of hybrid ac/dc power systems could vary due to the fluctuations of power demands and generations, the linearized model should be updated and the variation range of Sigmoid functions (16) and (17) can be further calculated. The updating procedure can be performed by the transmission system operator (TSO) if the steady-state equilibrium changes dramatically, and then the new variation range can be sent to the AVSG controller. Although the steady-state equilibrium is changing all the time, the parameters could be updated at regular intervals, e.g., 5 mins, as the equilibrium does not always change dramatically. Hence, the TSO has enough time to update the linearized model and controller parameters.

V. Case Study I

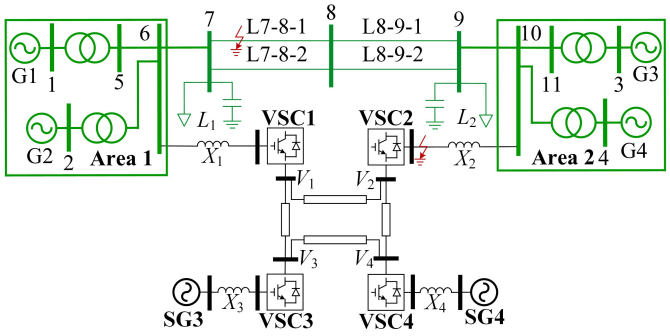

Fig. 11. 2-area 4-machine system with VSC-MTDC system.

To validate the effectiveness of the proposed VSG controller, the test system shown in Fig. 11 is developed in DIgSILENT/PowerFactory. VSC1 and VSC2 connect with Kundur's 2-area 4-machine system via Bus 6 and Bus10, and VSC3 and VSC4 connect with two equivalent synchronous generators, respectively. The AVM model of VSC-stations with a built-in reactor on the ac side is used. The proposed AVSG controller is applied in VSC1 and VSC2, and VSC3 and VSC4 are controlled by $P - V$ droop controller for dc voltage regulation. The synchronous generators G1 − 4 are modeled by the detailed 6-order model. Speed governor and excitation system of each generator are modeled by TGOV1 model [29] and IEEE type AC4A model [30]. The equivalent π model is used for modeling the ac transmission lines and dc cables. The load L_1 and L_2 are $P_{L1} = 1267$MW, $Q_{L1} = 100$Mvar and $P_{L2} = 2267$MW, $Q_{L2} = 100$Mvar, respectively. The parameters of the test system including the proposed VSG controller, synchronous generators, dc cables, ac transmission lines, and transformers are given in Table IV and other parameters of the 2-area 4-machine system can be referred to [31]. The simulation time-step is 0.01s.

TABLE IV
Parameters of the Test System

VSC-station parameters		
Rated Power: 800MVA		Resistive loss factor: 242mΩ
Rated ac voltage: 220kV		No-load losses: 3000kW
Rated dc voltage: 800kV		Equivalent arm inductance: 45mH
Short-circuit impedance: 15%		Equivalent dc capacitor: 100μF
Copper losses: 2400kW		$X1-4: 12.1229\Omega$
Control strategy		
VSC1	AVSG	$P_0 = 300$MW, $Q_0 = 0$Mvar
VSC2	AVSG	$P_0 = 500$MW, $Q_0 = 0$Mvar
VSC3	$P - V$	$P_0 = -418.2$MW, $V_0 = 800$kV
VSC4	$P - V$	$P_0 = -400$MW, $V_0 = 799.929$kV
AVSG parameters		
$H_{v,1} = 2$s, $H_{v,2} = 4$s, $K_{v\omega 0} = 5$p.u., $K_{vv0} = 0$p.u.		
$\lvert\frac{d\omega_v}{dt}\rvert_t = 0.001$p.u., $\lvert\Delta V\rvert_t = 0.001$p.u.		
$\Delta\omega_{\max} = \pm 0.01$p.u., $\Delta V_{\max} = \pm 0.02$p.u.		
$K_{v\omega,\max} = 100$p.u., $K_{v\omega,\min} = 0$p.u.		
$K_{vv,\max} = 50$p.u., $K_{vv,\min} = 0$p.u.		
$k_{r\omega,1} = 20000$, $k_{r\omega,2} = 23000$, $k_{rv,1} = 1000$, $k_{rv,2} = 1200$		
$x_{\omega 0,1} = 1.472 \times 10^{-4}$, $x_{\omega 0,2} = 1.28 \times 10^{-4}$, $x_{v0,1} = 0.0177$, $x_{v0,2} = 0.0147$		
Synchronous generator parameters		
Rated Power: 900MVA		Transient reactance q-axis: 0.55p.u.
Rated voltage: 20kV		Subtransient reactance d-axis: 0.25p.u.
Inertia constant: 6.5s		Subtransient reactance q-axis: 0.55p.u.
Stator leakage reactance: 0.2p.u.		Transient time constant d-axis: 1.333s
Synchronous reactance d-axis: 1.8p.u.		Transient time constant q-axis: 0.129s
Synchronous reactance q-axis: 1.7p.u.		Subtransient time constant d-axis: 0.025s
Transient reactance d-axis: 0.3p.u.		Subtransient time constant q-axis: 0.023s
Transmission line parameters in per unit length		
AC		**DC**
Resistance: 0.0529Ω/km		Resistance: 0.0114Ω/km
Inductance: 1.40322mH/km		Inductance: 0.9356mH/km
Capacitance: 0.00806μF/km		Capacitance: 0.0123μF/km
Transformer parameters		
Rated power: 900MVA		Short circuit voltage: 15%
Rated high voltage: 230kV		Copper losses: 5500kW
Rated low voltage: 20kV		

The oscillation modes which the VSG participate in are identified by modal analysis. As can be observed in Table. V, three LFOs are related with the VSG controller. The mode

TABLE V
CRITICAL OSCILLATORY MODES

Mode number	Eigenvalue	ζ	ω_o(Hz)
1	-0.101±2.999	0.034	0.477
2	-0.675±9.837	0.069	1.562
3	-0.727±10.194	0.071	1.622

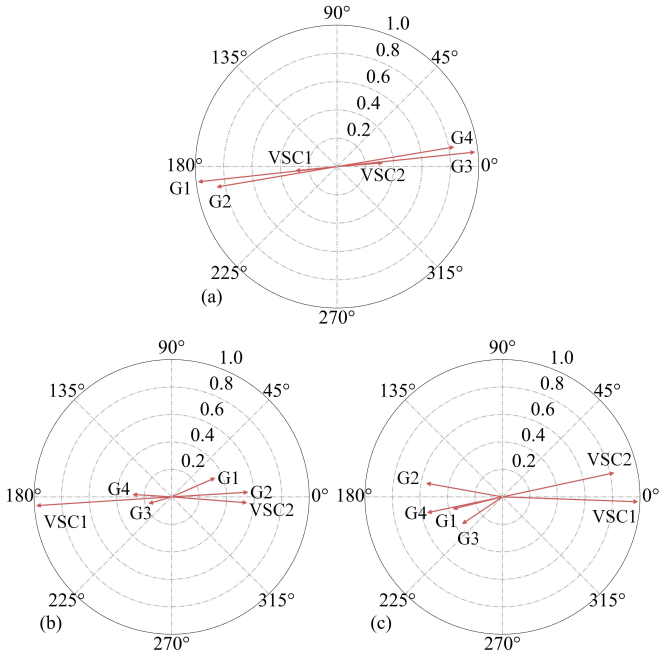

Fig. 12. Mode shapes. (a) Mode1; (b) Mode2; (c) Mode3.

shapes of these LFOs are shown in Fig. 12. One can find that the VSG controllers participate in two local modes and one inter-area mode. To test the damping performance of the proposed AVSG, two events are considered:

a) A three-phase short-circuit fault on the transmission line L7-8-1 occurs at $t = 1$s and is cleared at $t = 1.1$s;
b) A three-phase short-circuit fault near the ac terminal of VSC2 occurs at $t = 1$s and is cleared at $t = 1.5$s;

A. Control Performance under Short-circuit Fault on Transmission Line L 7-8-1

The system responses when VSC1 and VSC2 are controlled by the proposed AVSG, VSG with alternating moment of inertia (AMI) proposed in [15], the classical VSG, and the $P-V$ droop controller are given in Figs. 13−15. The $P-V$ droop controller has no damping ability because of its decoupling control between ac and dc side. Thus dc voltage oscillation is not triggered. The classical VSG has a poor damping performance on oscillations in ac grids. The VSC-MTDC system suffers from severe dc voltage oscillation, which threatens the system stability and reduces the lifetime of dc components. AMI can somewhat improve the system damping but the dc voltage still oscillates for several seconds. When the proposed AVSG is applied in VSC1 and VSC2, the power oscillation on L7-8-1 and the rotor speed oscillation of

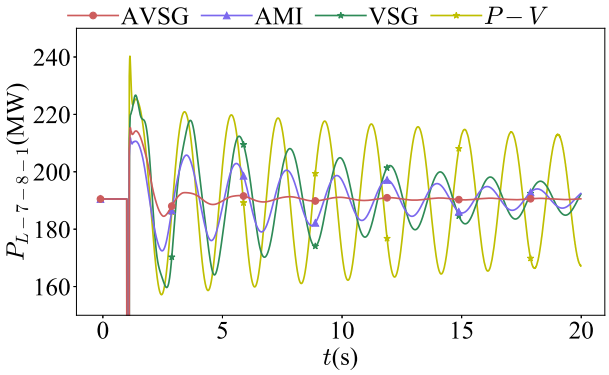

Fig. 13. Active power transmitted by L7-8-1

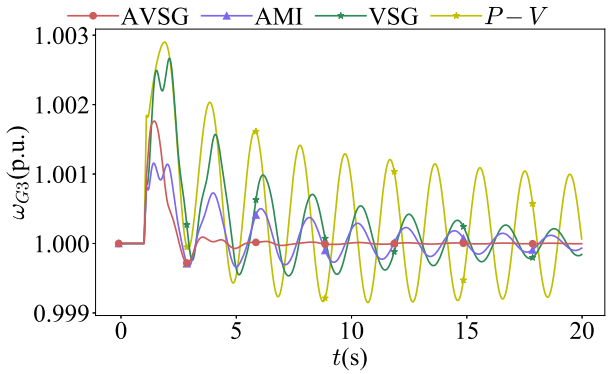

Fig. 14. Rotor speed of G3.

G3 are well-damped. The maximum dc voltage deviation is reduced and restores to zero quickly.

B. Control Performance under Short-circuit Fault Near VSC2

To investigate the low voltage ride through (LVRT) capacity of the AVSG controller, a three-phase short circuit fault close to the ac-terminal of VSC2 occurs at $t = 1$s and is cleared at $t = 1.5$s. During an ac grid fault near the VSC-MTDC system, the power output of the VSC-station is suppressed due to the voltage sags and the balance between the power injection and output of VSC-MTDC is broken. The imbalance power of dc grid will result in dc overvoltages in all the dc terminals [32].

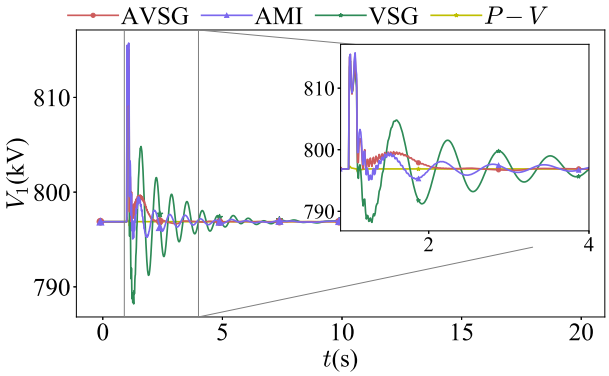

Fig. 15. DC voltage of VSC1.

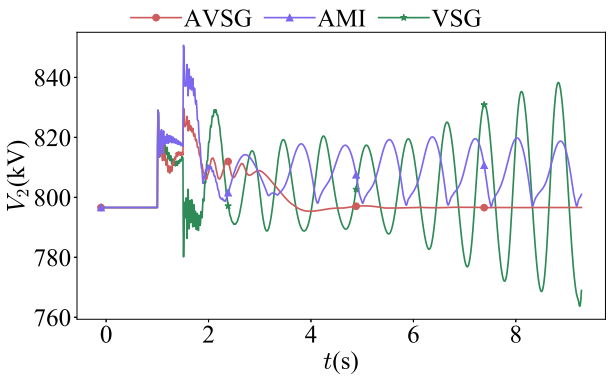

Fig. 16. DC voltage of VSC2.

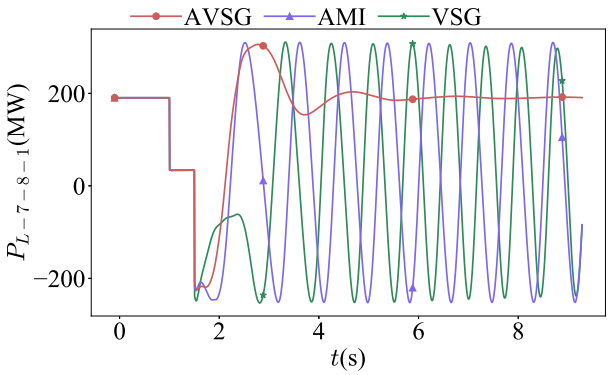

Fig. 17. Active power transmitted by L7-8-1

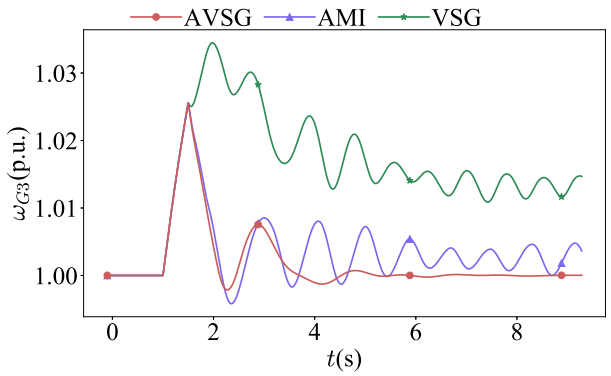

Fig. 18. Rotor speed of G3.

To avoid equipment damages during the fault period, the LVRT capacity is a major concern.

The system responses with different controllers (AVSG, AMI, and the classical VSG) applied in VSC1 and VSC2 are given in Figs. 16−18. As can be observed, the amplitude of dc voltage oscillation is increasing after the fault is cleared. Thus, the classical VSG cannot secure the system stability. AMI has poor LVRT capability as oscillations with equal amplitude are triggered in ac and dc side. The proposed AVSG could effectively dampen the oscillations in ac and dc side. The dc voltage, rotor speed and active power on the transmission lines restore to the initial value rapidly. Thus, the proposed AVSG has the best LVRT capacity among the other VSG controllers.

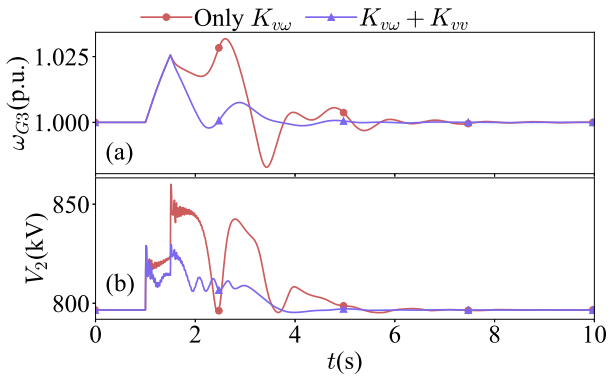

Fig. 19. The system responses of the proposed AVSG with and without the $P-V$ droop characteristic. (a) the rotor speed of G3; (b) the dc voltage of VSC2.

To further show the capability of different parts of the AVSG controller, the system responses of AVSG with and without the $P-V$ droop characteristic in (3) are shown in Fig. 19. When AVSG doesn't include the $P-V$ droop characteristic, only $K_{v\omega}$ is changeable and the dc voltage deviation and rotor oscillation are more serious than that when both the $K_{v\omega}$ and K_{vv} are adjusted.

VI. Case Study II

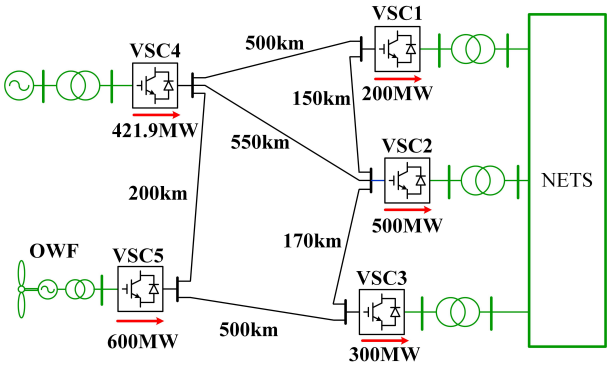

Fig. 20. 39-bus NETS with VSC-MTDC system.

To validate the effectiveness of the proposed VSG controller in a complex system, a test system including a 5-terminal VSC-MTDC system, two ac systems, and an OWF is used, as shown in Fig. 20. One ac system is the 39-bus New England Test System (NETS), which connects to the VSC-MTDC system via Bus20, Bus39, and Bus2. The equivalent ac grid is connected with VSC4. An offshore wind farm (OWF) with 150 Doubly fed Induction Generator (DFIG) based wind turbines is connected with VSC5. VSC1−VSC3 adopts the proposed AVSG controller. VSC4 employs the constant dc voltage control and VSC5 is operated in $|V_{ac}|-f$ control mode, which aims at maintaining the ac voltage magnitude and the frequency of the OWF [1]. The loads of the original NETS are magnified 1.164 times. The parameters of VSC-stations and dc cables are the same as that shown in Table IV. The topology and parameters of NETS can be referred to

TABLE VI
PARAMETERS OF THE TEST SYSTEM

Control strategy		
VSC1	AVSG	$P_0 = 200$MW, $Q_0 = 0$Mvar
VSC2	AVSG	$P_0 = 500$MW, $Q_0 = 0$Mvar
VSC3	AVSG	$P_0 = 300$MW, $Q_0 = 0$Mvar
VSC4	Constant dc voltage	$P_0 = -421.9$MW, $V_0 = 800$kV
VSC5	$\|V_{ac}\| - f$	$P_0 = -600$MW, $V_ac = 220$kV
AVSG parameters		
$H_{v,1} = 4$s, $H_{v,2} = 2$s, $H_{v,3} = 3$s		
$K_{v\omega 0} = 5$p.u., $K_{vv0} = 0$p.u., $\|\frac{d\omega_v}{dt}\|_t = 0.001$p.u., $\|\Delta V\|_t = 0.001$p.u.		
$\Delta\omega_{\max} = \pm 0.01$p.u., $\Delta V_{\max} = \pm 0.02$p.u.		
$K_{v\omega,\max} = 100$p.u., $K_{v\omega,\min} = 0$p.u.		
$K_{vv,\max} = 50$p.u., $K_{vv,\min} = 0$p.u.		
$k_{r\omega,1} = 20000$, $k_{r\omega,2} = 18000$, $k_{r\omega,3} = 23000$		
$k_{rv,1} = 800$, $k_{rv,2} = 1000$, $k_{rv,3} = 1200$		
$x_{\omega 0,1} = 1.472 \times 10^{-4}$, $x_{\omega 0,2} = 1.636 \times 10^{-4}$, $x_{\omega 0,3} = 1.28 \times 10^{-4}$		
$x_{v0,1} = 0.0222$, $x_{v0,2} = 0.0177$, $x_{v0,3} = 0.0148$		
Transformer parameters		
Rated power: 900MVA Rated high voltage: 345kV Rated low voltage: 220kV		Short circuit voltage: 10% Copper losses: 5000kW
DFIG parameters		
Rated power: 6MVA Rated voltage: 0.69kV Number of pole pairs: 2 Inertia constant: 0.376s Stator winding resistance: 0.01p.u.		Stator leakage reactance: 0.1p.u. Rotor resistance: 0.01p.u. Rotor leakage reactance: 0.1p.u. Magnetizing reactance: 3.5p.u.

[33]. Other parameters of the test system is given in Table VI.

TABLE VII
CRITICAL OSCILLATORY MODES

Mode number	Eigenvalue	ζ	ω_o(Hz)
1	-0.741±10.737	0.069	1.693
2	-0.462±10.193	0.045	1.622
3	-0.146±9.596	0.015	1.527
4	-0.357±5.838	0.061	0.929

The oscillation modes where VSG participate in are shown in Table. VII. Four LFOs are related with VSG controllers. The mode shapes of these LFOs are shown in Fig. 21. To test the damping performance of the proposed AVSG in the large-scale power system, a three-phase fault is applied on the transmission line L15−16 at $t = 1$s and is cleared at $t = 1.1$s. The system responses are shown in Fig. 22−23.

It can be observed from Fig. 22 that the proposed AVSG can damp the power oscillation on the transmission lines L6−7 and L9−39 much quicker than AMI and the classical VSG. The dc voltage variation of the VSC-MTDC system with different controllers are demonstrated in Fig. 23. During the fault period, the dc voltage deviation with the different controller is similar. However, the VSC-MTDC system suffers from dc voltage oscillations over a much longer time when AMI and the classical VSG are employed. Hence, the proposed AVSG can restrain both the oscillations in the ac and dc side

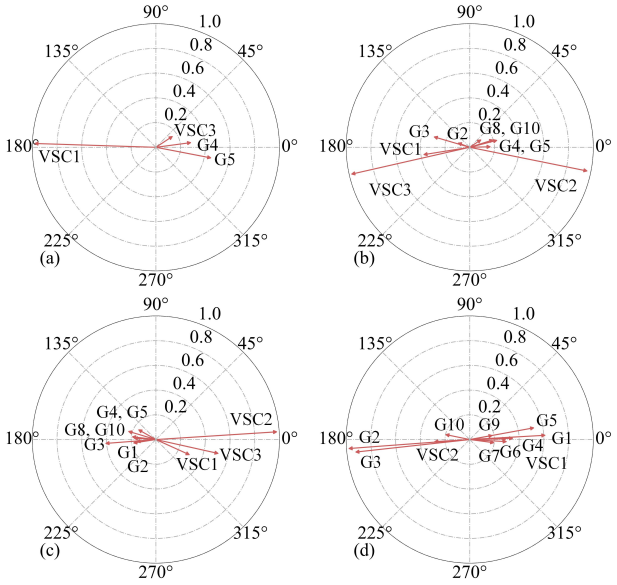

Fig. 21. Mode shapes. (a) Mode1; (b) Mode2; (c) Mode3; (d) Mode4.

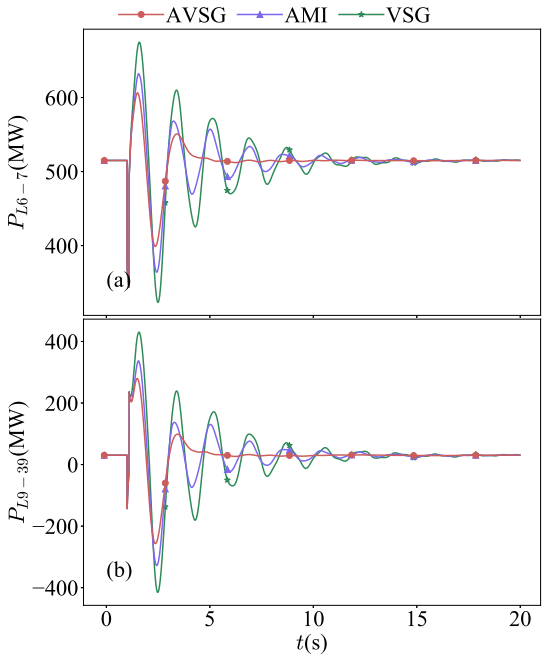

Fig. 22. The power oscillations on transmission lines. (a) L6−7; (b) L9−39.

and the stability of the entire hybrid ac/dc power systems is improved.

VII. CONCLUSIONS

This paper has investigated how to synthesize and tune the parameters of a virtual synchronous generator based controller for damping the ac-side low frequency oscillations. The negative impact of the classical VSG controller on dc-side voltage stability is also attenuated. The effectiveness of the proposed VSG was validated by nonlinear simulation. Results are summarized as follows:

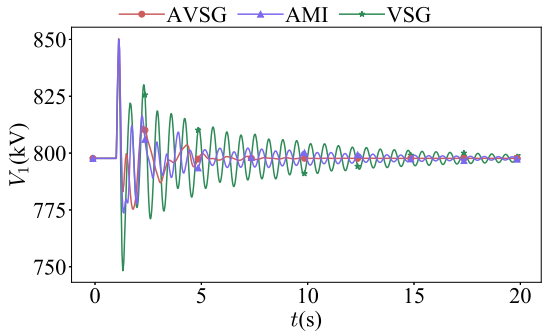

Fig. 23. The dc voltage of VSC1.

a) It was shown that the classical VSG controller could spread ac side oscillations to the dc side. Although large H_v can reduce the rate of change of frequency, but it also provokes a large resonant peak of the dc voltage and reduces the damping ratio of low frequency oscillatory modes. Thus, the inappropriate H_v is detrimental to system stability;
b) It was pointed out that increasing $K_{v\omega}$ and K_{vv} can strengthen the damping performance of the VSG controllers, and effectively suppress the resonance peaks of the dc voltage;
c) It was shown that the proposed AVSG controller can smoothly switch the $K_{v\omega}$ and K_{vv} in real-time to dampen the low frequency oscillations in the ac grid and thus the negative influence of VSG controllers on dc voltage stability is attenuated.

Since only the local information is used to dampen the oscillations, the global optimal control performance cannot be ensured by the proposed AVSG controller. Moreover, the stochastic change of system operating point poses a challenge to the controller parameter setting. The damping performance may be weakened due to the variation of system operating point. Future works will consider the robust controller design for improving the global dynamic performance and avoid the negative impact of the equilibrium variation on controller performance.

REFERENCES

[1] J. Liang, T. Jing, O. Gomis-bellmunt, J. Ekanayake, and N. Jenkins, "Operation and Control of Multiterminal HVDC Transmission for OffshoreWind Farms," *IEEE Transactions on Power Delivery*, vol. 26, no. 4, pp. 2596–2604, 2011.

[2] D. Van Hertem, O. Gomis-Bellmunt, and J. Liang, *HVDC Technology and Technology for Offshore Grids*. IEEE, 2016. [Online]. Available: https://ieeexplore.ieee.org/document/7435071

[3] N. A. Masood, N. Modi, and R. Yan, "Low inertia power systems: Frequency response challenges and a possible solution," *Proceedings of the 2016 Australasian Universities Power Engineering Conference, AUPEC 2016*, 2016.

[4] J. Driesen and K. Visscher, "Virtual synchronous generators," *IEEE Power and Energy Society 2008 General Meeting: Conversion and Delivery of Electrical Energy in the 21st Century, PES*, pp. 1–3, 2008.

[5] Q. C. Zhong and G. Weiss, "Synchronverters: Inverters that mimic synchronous generators," *IEEE Transactions on Industrial Electronics*, vol. 58, no. 4, pp. 1259–1267, 2011.

[6] M. Guan, W. Pan, J. Zhang, Q. Hao, J. Cheng, and X. Zheng, "Synchronous Generator Emulation Control Strategy for Voltage Source Converter (VSC) Stations," *IEEE Transactions on Power Systems*, vol. 30, no. 6, pp. 3093–3101, 2015.

[7] Y. Chen, R. Hesse, D. Turschner, and H. P. Beck, "Improving the grid power quality using virtual synchronous machines," *2011 International Conference on Power Engineering, Energy and Electrical Drives*, no. May, pp. 1–6, 2011. [Online]. Available: http://ieeexplore.ieee.org/lpdocs/epic03/wrapper.htm?arnumber=6036498

[8] T. Shintai, Y. Miura, and T. Ise, "Oscillation damping of a distributed generator using a virtual synchronous generator," *IEEE Transactions on Power Delivery*, 2014.

[9] Y. Hirase, K. Sugimoto, K. Sakimoto, and T. Ise, "Analysis of resonance in microgrids and effects of system frequency stabilization using a virtual synchronous generator," *IEEE Journal of Emerging and Selected Topics in Power Electronics*, vol. 4, no. 4, pp. 1287–1298, Dec 2016.

[10] L. Huang, H. Xin, and Z. Wang, "Damping low-frequency oscillations through vsc-hvdc stations operated as virtual synchronous machines," *IEEE Transactions on Power Electronics*, vol. 34, no. 6, pp. 5803–5818, June 2019.

[11] S. Dong and Y. C. Chen, "Adjusting Synchronverter Dynamic Response Speed via Damping Correction Loop," *IEEE Transactions on Energy Conversion*, vol. 32, no. 2, pp. 608–619, 2017.

[12] L. Huang, H. Xin, H. Yang, Z. Wang, H. Xie, S. Member, H. Xin, and H. Yang, "Interconnecting Very Weak AC Systems by Multiterminal VSC-HVDC Links with a Unified Virtual Synchronous Control," *IEEE Journal of Emerging and Selected Topics in Power Electronics*, vol. 6, no. 3, pp. 1041–1053, 2018.

[13] A. Asrari, M. Mustafa, M. Ansari, and J. Khazaei, "Impedance Analysis of Virtual Synchronous Generator-Based Vector Controlled Converters for Weak AC Grid Integration," *IEEE Transactions on Sustainable Energy*, vol. PP, no. c, pp. 1–1, 2019.

[14] M. A. Torres L., L. A. Lopes, L. A. Morán T., and J. R. Espinoza C., "Self-tuning virtual synchronous machine: A control strategy for energy storage systems to support dynamic frequency control," *IEEE Transactions on Energy Conversion*, vol. 29, no. 4, pp. 833–840, 2014.

[15] J. Alipoor, Y. Miura, and T. Ise, "Power system stabilization using virtual synchronous generator with alternating moment of inertia," *IEEE Journal of Emerging and Selected Topics in Power Electronics*, vol. 3, no. 2, pp. 451–458, 2015.

[16] J. Alipoor, Y. Miura, and T. Ise, "Stability assessment and optimization methods for microgrid with multiple vsg units," *IEEE Transactions on Smart Grid*, vol. 9, no. 2, pp. 1462–1471, March 2018.

[17] D. Li, Q. Zhu, S. Lin, and X. Y. Bian, "A Self-Adaptive Inertia and Damping Combination Control of VSG to Support Frequency Stability," *IEEE Transactions on Energy Conversion*, vol. 32, no. 1, pp. 2016–2017, 2017.

[18] F. Wang, L. Zhang, X. Feng, and H. Guo, "An Adaptive Control Strategy for Virtual Synchronous Generator," *IEEE Transactions on Industry Applications*, vol. 54, no. 5, pp. 5124–5133, 2018.

[19] J. Peralta, H. Saad, S. Dennetière, J. Mahseredjian, and S. Nguefeu, "Detailed and averaged models for a 401-level MMC-HVDC system," *IEEE Transactions on Power Delivery*, vol. 27, no. 3, pp. 1501–1508, 2012.

[20] H. Saad, S. Dennetiere, J. Mahseredjian, P. Delarue, X. Guillaud, J. Peralta, and S. Nguefeu, "Modular multilevel converter models for electromagnetic transients," *IEEE Transactions on Power Delivery*, vol. 29, no. 3, pp. 1481–1489, 2014.

[21] W. Wang, M. Barnes, O. Marjanovic, and O. Cwikowski, "Impact of DC breaker systems on multiterminal VSC-HVDC stability," *IEEE Transactions on Power Delivery*, vol. 31, no. 2, pp. 769–779, 2016.

[22] Y. Li, G. Tang, J. Ge, Z. He, H. Pang, J. Yang, and Y. Wu, "Modeling and Damping Control of Modular Multilevel Converter Based DC Grid," *IEEE Transactions on Power Systems*, vol. 33, no. 1, pp. 723–735, 2017.

[23] S. Saeid, H. Yazdi, K. Rouzbehi, J. I. Candela, J. Milimonfared, P. Rodriguez, S. S. H. Yazdi, K. Rouzbehi, J. Ignacio Candela, J. Milimonfared, and P. Rodriguez, "Flexible HVDC Transmission Systems Small Signal Modelling : A case study on CIGRE Test MT-HVDC Grid," *Proceedings IECON 2017 - 43rd Annual Conference of the IEEE Industrial Electronics Society*, pp. 256–262, 2017.

[24] J. Liu, Y. Miura, and T. Ise, "Comparison of dynamic characteristics between virtual synchronous generator and droop control in inverter-based distributed generators," *IEEE Transactions on Power Electronics*, vol. 31, no. 5, pp. 3600–3611, May 2016.

[25] X. Meng, J. Liu, and Z. Liu, "A generalized droop control for grid-supporting inverter based on comparison between traditional droop control and virtual synchronous generator control," *IEEE Transactions on Power Electronics*, vol. 34, no. 6, pp. 5416–5438, June 2019.

[26] A. Yazdani and R. Iravani, *Voltage-sourced converters in power systems*. Wiley Online Library, 2010, vol. 34.

[27] E. Prieto-Araujo, F. D. Bianchi, A. Junyent-Ferré, O. Gomis-Bellmunt, S. Member, and O. Gomis-Bellmunt, "Methodology for droop control dynamic analysis of multiterminal VSC-HVDC grids for offshore wind farms," *IEEE Transactions on Power Delivery*, vol. 26, no. 4, pp. 2476–2485, 2011.
[28] R. Eriksson, J. Beerten, M. Ghandhari, and R. Belmans, "Optimizing DC voltage droop settings for AC/DC system interactions," *IEEE Transactions on Power Delivery*, vol. 29, no. 1, pp. 362–369, 2014.
[29] P. S. D. P. Committee *et al.*, "Dynamic models for turbine-governors in power system studies," *IEEE Power & Energy Society*, 2013.
[30] "Ieee recommended practice for excitation system models for power system stability studies," *IEEE Std 421.5-2016 (Revision of IEEE Std 421.5-2005)*, pp. 1–207, Aug 2016.
[31] P. Kundur, N. J. Balu, and M. G. Lauby, *Power system stability and control*. McGraw-hill New York, 1994.
[32] B. Silva, C. L. Moreira, H. Leite, and J. A. Pecas Lopes, "Control strategies for AC fault ride through in multiterminal HVDC grids," *IEEE Transactions on Power Delivery*, vol. 29, no. 1, pp. 395–405, 2014.
[33] M. Pai, *Energy function analysis for power system stability*. Springer Science & Business Media, 2012.

Weiyu Wang (S'16) was born in Shanxi, China, in 1992. He received the B.S. degree from the College of Electrical and Information Engineering, Hunan University, Changsha, China, in 2014. Since 2014, he has been working toward the Ph.D. degree in the College of Electrical and Information Engineering, Hunan University, Changsha, China. His research interests include the stability analysis and control of hybrid ac/dc power systems.

Lin Jiang (M'00) received the B.S. and M.S. degrees from Huazhong University of Science and Technology (HUST), China, in 1992 and 1996; and the Ph.D. degree from the University of Liverpool, UK, in 2001, all in Electrical Engineering. He worked as a Postdoctoral Research Assistant in the University of Liverpool from 2001 to 2003, and Postdoctoral Research Associate in the Department of Automatic Control an Systems Engineering, the University of Sheffield from 2003 to 2005. He was a Senior Lecturer at the University of Glamorgam from 2005 to 2007 and moved to the University of Liverpool in 2007. Currently, he is a Reader in The University of Liverpool. His current research interests include control and analysis of power system, smart grid, and renewable energy.

Yijia Cao (M'98–SM'13) was born in Hunan, China, in 1969. He received the Graduation degree from Xi'an Jiaotong University, Xi'an, China in 1988, and the M.Sc. and Ph.D. degrees from Huazhong University of Science and Technology (HUST), Wuhan, China, in 1991 and 1994, respectively. From September 1994 to April 2000, he was a Visiting Research Fellow and a Research Fellow with Loughborough University, Liverpool University, and the University of the West England, U.K. From 2000 to 2001, he was employed as a Full Professor with HUST, and from 2001 to 2008, he was employed as a Full Professor with Zhejiang University, China. He was appointed as the Deputy Dean of the College of Electrical Engineering, Zhejiang University in 2005. He is currently a Full Professor and the President of the Changsha University of Science and Technology, Changsha, China. His research interests are power system stability control and the application of intelligent systems in power systems.

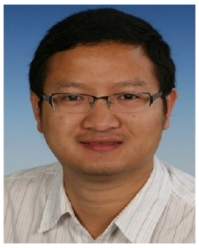

Yong Li (S'09–M'12–SM'14) was born in Henan, China, in 1982. He received the B.Sc. and Ph.D. degrees from the College of Electrical and Information Engineering, Hunan University (HNU), Changsha, China, in 2004 and 2011, respectively. Since 2009, he has been working as a Research Associate at the Institute of Energy Systems, Energy Efficiency, and Energy Economics, Technical University of Dortmund, Dortmund, Germany, from where he received the second Ph.D. degree in June 2012. Since 2014, he has been a Full Professor of electrical engineering at HNU. His current research interests include ac/dc energy conversion systems, analysis and control of power quality, and HVDC and FACTS technologies.